Simulation of Directional Microphones in Digital Waveguide Mesh-based Models of Room Acoustics

Hüseyin Hacıhabiboğlu, *Member, IEEE*, Banu Günel, *Member, IEEE*, and Zoran Cvetković, *Senior Member, IEEE*

***Abstract*—Digital waveguide mesh (DWM) models are time-domain numerical methods providing computationally simple solutions for wave propagation problems. They have been used in various acoustical modeling and audio synthesis applications including synthesis of musical instrument sounds and speech, and modeling of room acoustics. A successful model of room acoustics should be able to account for source and receiver directivity. Methods for the simulation of directional sources in DWM models were previously proposed. This article presents a method for the simulation of directional microphones in DWM-based models of room acoustics. The method is based on the directional weighting of the microphone response according to the instantaneous direction of incidence at a given point. The direction of incidence is obtained from instantaneous intensity that is calculated from local pressure values in the DWM model. The calculation of instantaneous intensity in DWM meshes and the directional accuracy of different mesh topologies is discussed. An intensity-based formulation for the response of a directional microphone is given. Simulation results for an actual microphone with frequency-dependent, non-ideal directivity function are presented.**

***Index Terms*—Microphones, room acoustics, finite difference methods, digital waveguide mesh, acoustic intensity.**

I. INTRODUCTION

DIGITAL waveguide mesh (DWM) models are numerical solvers of the wave equation providing second-order accurate solutions in two or higher dimensional problems [1]. Simulation of room acoustics using wave-theoretical models such as the DWM is particularly useful, as these models readily simulate wave-related phenomena such as obstruction and diffraction [2]. Simulation of these phenomena using geometry-based models of room acoustics requires extra computational effort [3], [4]. In many room modeling and simulation applications involving DWMs, both the source and receiver models are omnidirectional [5]–[7]. However, real acoustical sources and receivers are never perfectly omnidirectional. In order to obtain more realistic simulations, microphone and source directivities have to be modeled.

Recently, a method for simulating broadband, frequency-dependent directional sources was proposed for DWM-based models of room acoustics [8], [9]. The method is based on the weighting of the simulated wave front using frequency-dependent source directivity data. It is possible to accurately simulate sources with analytic (such as a dipole source) and empirical (such as human mouth or loudspeaker) directivity functions using that method. Subsequently, another method based on multipole synthesis for simulating directional sources in DWM models was proposed [10].

Simulation of directional microphones on DWM models was addressed indirectly in [11], [12]. However, those works investigated the simulation of differential microphone arrays with the aim of obtaining signals that can be used for encoding the acoustics of the room using second-order Ambisonics, and not modeling and simulating actual directional microphones per se.

A method for simulating directional microphones in DWM models is presented in this article. The proposed method is based on the numerical calculation of instantaneous intensity at the microphone position to determine the instantaneous local direction of the simulated sound field. The instantaneous response of the directional microphone is obtained based on the instantaneous intensity and the direction estimate.

Section II provides an overview of DWM models. A method for the calculation of instantaneous acoustic intensity in DWM models is given in Section III. Section IV explains the method for simulating directional microphones in DWM models together with a discussion of microphone directivity and its relation to acoustic intensity. Section V presents the simulation of a real directional microphone using tabulated directivity data as an example. Section VI concludes the paper.

II. DIGITAL WAVEGUIDE MESH MODELS

Wave propagation problems for acoustical resonators with simple geometries can usually be solved theoretically. However, a closed-form theoretical solution is generally not possible for acoustical modeling problems with complex geometries. Numerical methods that solve the wave equation locally can be used in such propagation problems. Finite element method (FEM) [13], boundary element method (BEM) [14], and finite-difference methods [15]–[17] are widely used for this purpose.

Manuscript received February 4, 2009, revised April 10, 2009; The first and third authors are funded by the Engineering and Physical Sciences Research Council (EPSRC) Research Grant EP/F001142/1. The second author is funded by VISNET II, a European Network of Excellence (http://www.visnetnoe.org), under the European Commission IST FP6 programme. The associate editor coordinating the review of this manuscript and approving it for publication was Prof. Stephen J. Elliott.

H. Hacıhabiboğlu and Z. Cvetković are with Centre for Digital Signal Processing Research (CDSPR), Division of Engineering, King's College London, Strand, London, WC2R 2LS, United Kingdom (e-mail: huseyin.hacihabiboglu@kcl.ac.uk; zoran.cvetkovic@kcl.ac.uk).

B. Günel is with Multimedia and DSP Research Group (I-Lab), Centre for Communication Systems Research (CCSR), University of Surrey, Guildford, GU2 7XH, United Kingdom (e-mail: b.gunel@surrey.ac.uk).

Publisher Item Identifier XX.XXXX/XXXXX.XXXX.XXXXXX

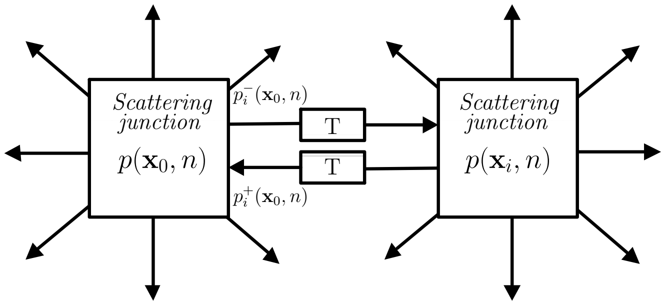

Fig. 1. Two DWM scattering junctions positioned at $\mathbf{x}_0$ and $\mathbf{x}_i$ connected by a bidirectional delay of T. The incoming and outgoing wave variables, $p_i^-(\mathbf{x}_0, n)$ and $p_i^-(\mathbf{x}_0, n)$ are shown.

Digital waveguide (DWG) modeling is a time-domain numerical method based on the concept of wave scattering. DWG models were originally devised for solving one-dimensional wave propagation problems such as on vibrating strings [18], [19]. They have been used in music [20], [21] and speech synthesis applications [22], [23]. DWG models consist of two-port junctions interconnected via bidirectional delay elements. The computational scheme has two consecutive steps that are carried out iteratively. In the first step, the incoming wave variables at the junction are scattered to obtain the outgoing wave variables. In the second step the calculated outgoing wave variables are propagated to the neighboring junctions. This provides a traveling wave, or *d'Alembert* solution of the wave equation.

DWG modeling can be generalized to two and three dimensions for simulating wave propagation in acoustical resonators such as drum membranes [24], [25] and rooms [5]–[9], [26]. Digital waveguide mesh (DWM) is the name given to these multidimensional models due to the scheme being operated on a multidimensional mesh.

Like DWG models, DWM models consist of multiport junctions interconnected via bidirectional delay elements. At any given instant, a given multiport junction with M neighbors, positioned at $\mathbf{x}_0$ will have incoming wave variables, $p_i^+(\mathbf{x}_0, n)$, and outgoing wave variables, $p_i^-(\mathbf{x}_0, n)$, at its port with the index i, connected to the neighboring junction positioned at $\mathbf{x}_i$ (see Fig. 1). These wave variables and the junction pressure, $p(\mathbf{x}_0, n)$ are related as follows [1]:

$$p(\mathbf{x}_0, n) = \frac{2}{Y_t} \sum_{i=1}^{M} Y_i p_i^+(\mathbf{x}_0, n), \tag{1}$$

$$p_i^-(\mathbf{x}_0, n) = p(\mathbf{x}_0, n) - p_i^+(\mathbf{x}_0, n), \tag{2}$$

where Y_i is the admittance of the i^{th} port and $Y_t = \sum_{i=1}^{M} Y_i$ is the total admittance. This operation is called the *scattering pass*.

The calculated outgoing wave variable at junction N is propagated to junction K using the following relation:

$$p_N^+(\mathbf{x}_K, n) = p_K^-(\mathbf{x}_N, n-1). \tag{3}$$

In other words, the outgoing wave variable of junction N at its port connected to the junction K is the incoming wave variable at the next time step for the latter. This operation is called the *propagation step*.

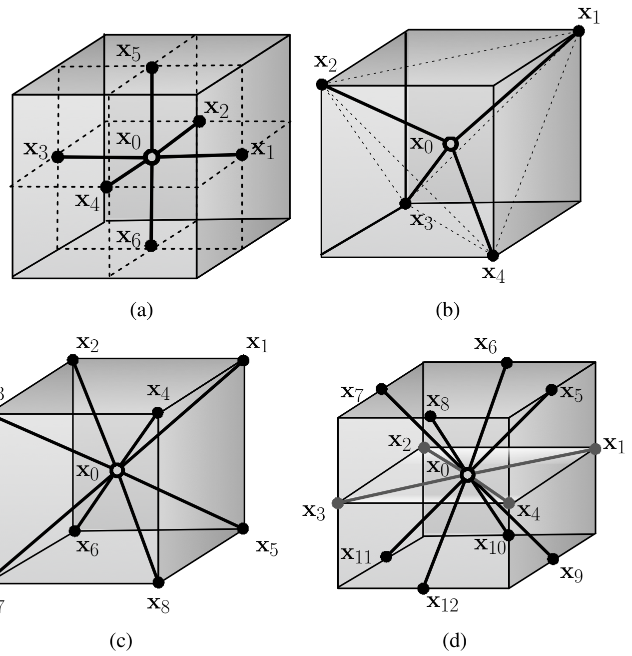

Fig. 2. Uniform 3D mesh topologies: (a) cubic ($M = 6$), (b) tetrahedral ($M = 4$), (c) body-centered cubic (BCC) ($M = 8$), and (d) cubic close-packed (CCP) ($M = 12$). The positions of the central junction, $\mathbf{x}_0$, and neighboring junctions, $\mathbf{x}_i$ are shown.

The scattering pass can be written as a matrix operation [1] such that,

$$\mathbf{p}^-(\mathbf{x}_0, n) = \mathbf{S}\ \mathbf{p}^+(\mathbf{x}_0, n) \tag{4}$$

where $\mathbf{S} = [2Y_i/Y_t]_{M\times M} - \mathbf{I}$ is called the *scattering matrix*, and $\mathbf{p}^+(\mathbf{x}_0, n)$ and $\mathbf{p}^-(\mathbf{x}_0, n)$ are the incoming and outgoing wave variable vectors. If the junction is situated in a homogenous medium the scattering matrix can be expressed as:

$$\mathbf{S} = \frac{2}{M}\mathbf{J}_M - \mathbf{I} \tag{5}$$

where $\mathbf{J}_M$ is the $M \times M$ matrix of ones and $\mathbf{I}$ is the $M \times M$ identity matrix. In this case the scattering matrix is a unitary matrix, i.e. $\mathbf{S^T S} = \mathbf{I}$ and the junction is lossless.

The DWM formulation is based on the assumption that the space is uniformly sampled and the distances between neighboring junctions are equal throughout the mesh. For 3D DWM models the spatial sampling period, r is related to the temporal sampling frequency, f_s by:

$$r = c\sqrt{3}/f_s, \tag{6}$$

where c is the nominal wave propagation speed on the mesh. For room acoustics modeling, r should be selected in such a way that the wave speed on the mesh is equal to the speed of sound in the air, $c_{sound} \approx 344$ m/s. For a sampling frequency of $f_s = 44.1$ kHz, the spatial sampling period is $r \approx 1.35$ cm. The bandwidth of a DWM model has a theoretical upper bound of $0.25\, f_s$ [27] but the actual bandwidth is generally lower [28].

There is a limited number of uniform sampling schemes (i.e. mesh topologies) in three dimensions. These are cubic, tetrahedral, body-centered cubic (BCC), and cubic close-packed (CCP) topologies [29]. Fig. 2 shows these topologies. As may be observed, a junction in cubic, tetrahedral, BCC, and CCP topologies, has 6, 4, 8, and 12 neighbors, respectively. These different topologies have different advantages in terms of directional dispersion [27], [29], [30], computational complexity [31], accuracy of numerical derivatives [32], and computational efficiency [29].

III. Calculation of Instantaneous Intensity in DWM Models

A. Calculation of instantaneous intensity

Acoustic intensity is a measure of the energy flow in an acoustical field. The instantaneous direction of the energy flow at a given point is coincident with the instantaneous intensity vector at that point. Let us consider the sound field at a given point, $\mathbf{x}$, in 3D space. The instantaneous intensity vector is defined as the product of pressure and velocity components:

$$\mathbf{I}(\mathbf{x}, t) = p(\mathbf{x}, t)\mathbf{v}(\mathbf{x}, t). \tag{7}$$

The velocity component can be obtained using the following approximation:

$$\mathbf{v}(\mathbf{x}, t+T) \approx \mathbf{v}(\mathbf{x}, t) + T\,\frac{\partial}{\partial t}\mathbf{v}(\mathbf{x}, t), \tag{8}$$

where the time derivative of velocity is proportional to the pressure gradient [33] such that

$$\frac{\partial}{\partial t}\mathbf{v}(\mathbf{x}, t) = -\frac{1}{\rho_0}\nabla p(\mathbf{x}, t). \tag{9}$$

If we further assume that the acoustic medium is homogenous and quiescent such that $\mathbf{v}(\mathbf{x}, 0) = 0$, the pressure gradient,

$$\nabla p(\mathbf{x}_J, t) = \left[\frac{\partial p}{\partial x}\ \frac{\partial p}{\partial y}\ \frac{\partial p}{\partial z}\right]_{x=\mathbf{x}_J}, \tag{10}$$

can be used to calculate the velocity at a given position $\mathbf{x}_J$ at any time instant.

A DWM model provides a discrete time and space solution and it is not possible to obtain the analytic gradient of the underlying continuous time pressure function. However, numerical gradients, which provide discrete-space approximations of the analytic gradients, can be obtained in different DWM topologies [32].

Let us have a central junction positioned at $\mathbf{x}_0 \in \mathbb{R}^3$ with M neighboring junctions positioned at $\{\mathbf{x_i} \in \mathbb{R}^3 : i = 1 \cdots M\}$ on a 3D mesh grid. Let us also define the 3D position vectors, $\overline{\mathbf{r}_i}$ such that:

$$\overline{\mathbf{r}_i} = \mathbf{x}_i - \mathbf{x}_0 = r\,\hat{\mathbf{u}}_i, \tag{11}$$

where $\hat{\mathbf{u}}_i = [u_{i,x}\ u_{i,y}\ u_{i,z}]$ for $i = 1 \cdots M$ is the unit vector in the direction of the neighboring junction and r is the common interjunction distance (i.e. spatial sampling period). The unit vector $\hat{\mathbf{u}}_i$ in spherical coordinates can be represented in the Cartesian coordinates as:

$$\begin{aligned} u_{i,x} &= \cos\phi_i \cos\theta_i, \\ u_{i,y} &= \cos\phi_i \sin\theta_i, \\ u_{i,z} &= \sin\phi_i, \end{aligned} \tag{12}$$

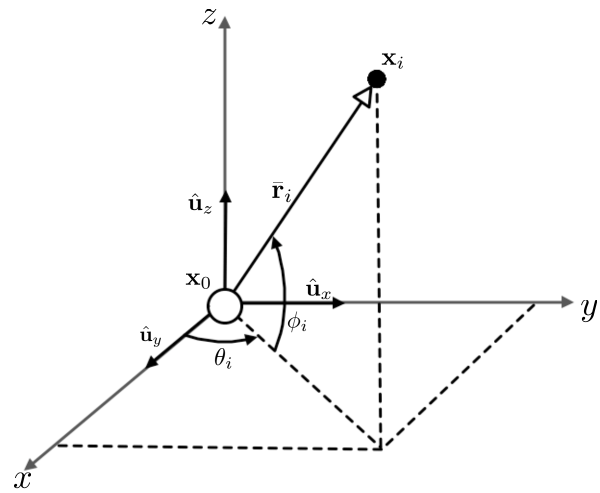

Fig. 3. Geometry of the problem. $\mathbf{x}_0$, $\mathbf{x}_i$: Positions of the central and neighboring junctions, $\bar{\mathbf{r}}_i$: position vector, $\hat{\mathbf{u}}_x$, $\hat{\mathbf{u}}_y$, $\hat{\mathbf{u}}_z$: unit vectors in the x, y, and z directions, and θ_i, ϕ_i: angular coordinates of the neighboring junction.

where $\{\theta_i\}$ and $\{\phi_i\}$ represent the angular coordinates of the spherical coordinate system. Fig. 3 shows the geometry of the problem.

For a three dimensional, real, differentiable function, $p(\mathbf{x})$, sampled at the described points, a first-order approximation of the directional derivatives can be obtained for the central junction positioned at $\mathbf{x}_0$ such that:

$$D_{\hat{\mathbf{u}}_i} p(\mathbf{x}_0) = \left[p(\mathbf{x}_i) - p(\mathbf{x}_0)\right]/r, \tag{13}$$

where $D_{\hat{\mathbf{u}}_i}$ denotes the directional derivative of $p(\mathbf{x})$ along the direction of the vector from $\mathbf{x}_0$ to $\mathbf{x}_i$.

This provides an approximation of the pressure gradient, $\nabla p(\mathbf{x})$, projected in the direction of $\hat{\mathbf{u}}_i$ such that:

$$\nabla p(\mathbf{x})|_{\mathbf{x}=\mathbf{x}_0} \cdot \hat{\mathbf{u}}_i \simeq D_{\hat{\mathbf{u}}_i} p(\mathbf{x}_0). \tag{14}$$

The ensemble of these approximations can be expressed as a set of linear equations by:

$$\mathbf{D}p(\mathbf{x}_0) \simeq \mathbf{U}\ \mathbf{d}p(\mathbf{x}_0), \tag{15}$$

where

$$\mathbf{D}p(\mathbf{x}_0) = \left[D_{\hat{\mathbf{u}}_1} p(\mathbf{x}_0)\ D_{\hat{\mathbf{u}}_2} p(\mathbf{x}_0) \cdots D_{\hat{\mathbf{u}}_M} p(\mathbf{x}_0)\ \right]^{\mathbf{T}}, \tag{16}$$

$$\mathbf{U} = \begin{bmatrix} u_{1,x} & u_{1,y} & u_{1,z} \\ u_{2,x} & u_{2,y} & u_{2,z} \\ \vdots & \vdots & \vdots \\ u_{M,x} & u_{M,y} & u_{M,z} \end{bmatrix}, \tag{17}$$

$$\mathbf{d}p(\mathbf{x}_0) = \left[\ \frac{\partial p}{\partial x}\ \ \frac{\partial p}{\partial y}\ \ \frac{\partial p}{\partial z}\ \right]^{\mathbf{T}}. \tag{18}$$

For uniform 3D mesh topologies the number of a junction's neighbors $M > 3$ and the system of linear equations will be overdetermined. The optimal solution for $\mathbf{d}p(\mathbf{x}_0)$ in the least squares sense can be obtained as:

$$\mathbf{d}p(\mathbf{x}_0) = \mathbf{U}^{+}\mathbf{D}p(\mathbf{x}_0), \tag{19}$$

where the inverse projection matrix, $\mathbf{U}^{+}$, is the Moore-Penrose pseudoinverse of the matrix $\mathbf{U}$ such that $\mathbf{U}^{+}\mathbf{U} = \mathbf{I}$. Each DWM topology has a different inverse projection matrix. Once the first-order approximation of the pressure gradient, $\mathbf{d}p(\mathbf{x})$, is calculated, the velocity and the intensity can be obtained from (8) and (7), respectively.

The horizontal and vertical angles, (θ_n, ϕ_n), of the sound field at the given junction and discrete-time instant can be calculated as:

$$\phi_n = \arcsin\left(\frac{\mathbf{I}\cdot\hat{\mathbf{u}}_z}{\|\mathbf{I}\|}\right),\ \theta_n = \arccos\left(\frac{\mathbf{I}\cdot\hat{\mathbf{u}}_x}{\|\mathbf{I}\|\cos\phi_n}\right). \quad (20)$$

It should be noted that the intensity calculation described above can be adapted to any DWM topology or to any 3D spatial sampling of an acoustical field. Thus the exposition given above is not specific to a single topology or computational scheme.

B. Accuracy of direction estimation

Different mesh topologies have different accuracies when calculating the pressure gradient. The magnitude errors of numerical gradients were discussed in [32]. It was shown that the tetrahedral topology provided the lowest magnitude error if the same spatial sampling period was used in all topologies. Cubic topology was shown to provide the lowest magnitude error if the mesh density (i.e. junctions per unit volume) was the same for all topologies.

The directional accuracy of the numerical gradient is also relevant in this paper. Similar to the magnitude errors encountered in the numerical calculation of pressure gradient, the accuracy of direction estimation will be frequency-dependent. Therefore, the analysis of different topologies for their accuracy of direction estimation is carried out in the spatial frequency-domain.

Let us express the pressure field, $p(\mathbf{x})$, in the frequency domain as $P(\bar{\omega})$, where $\bar{\omega} = [\omega_x\ \omega_y\ \omega_z]$ is the spatial frequency vector. Each point in the spatial frequency domain corresponds to a single spatial frequency vector and represents a monochromatic plane wave with the angular frequency $\omega_0 = \|\bar{\omega}\|/\sqrt{3}$ propagating in the opposite direction of that vector [34]. If we assume that the spatial sampling period (i.e. interjunction spacing) is r, the numerical derivatives in the directions of the neighboring junctions can be expressed in spatial frequency-domain by the 3D spatial Fourier transform as:

$$D_{\hat{\mathbf{u}}_i}p(\mathbf{x}) \xrightarrow{\mathcal{F}_{3D}} D_{\hat{\mathbf{u}}_i}P(\overline{\omega}) = \frac{1}{r}\left(e^{-jr\overline{\omega}\cdot\hat{\mathbf{u}}_i} - 1\right)P(\overline{\omega}). \quad (21)$$

Here, we used the shift theorem to express the pressure at the neighboring junction as a function of pressure at the central junction.

The numerical derivative vector in (16) can be expressed in the frequency domain as

$$\mathbf{P}_\Delta = [D_{\hat{\mathbf{u}}_1}P(\overline{\omega})\ D_{\hat{\mathbf{u}}_2}P(\overline{\omega})\cdots D_{\hat{\mathbf{u}}_M}P(\overline{\omega})\ ]^{\mathbf{T}}. \quad (22)$$

Then, the numerical gradient expressed in the spatial frequency domain can be obtained as

$$\mathbf{d}P(\overline{\omega}) = \mathbf{U}^{+}\mathbf{P}_\Delta. \quad (23)$$

The frequency domain expression for the actual gradient is:

$$\nabla p(\mathbf{x}) \xrightarrow{\mathcal{F}_{3D}} j\overline{\omega}P(\overline{\omega}). \quad (24)$$

The accuracy of direction estimation can be quantified by the angle between the actual and numerical gradients in the spatial frequency domain. The angle between two real valued vectors in $\mathbb{R}^N$ can be obtained using the scalar product of the vectors. However, frequency-domain vectors representing gradients are in $\mathbb{C}^N$. The angle between two complex vectors, $\mathbf{a},\mathbf{b} \in \mathbb{C}^N$, is defined as the Hermitian angle $\Theta_{\mathbf{H}}\{\mathbf{a},\mathbf{b}\}$ [35]:

$$\Theta_{\mathbf{H}}\{\mathbf{a},\mathbf{b}\} = \arccos\left|\frac{(\mathbf{a},\mathbf{b})_{\mathbf{C}}}{|\mathbf{a}|\,|\mathbf{b}|}\right|, \quad (25)$$

where $(\mathbf{a},\mathbf{b})_{\mathbf{C}} = \sum_{k=1}^{N} a_k^* b_k$ is the Hermitian product, and $|\mathbf{a}| = \sqrt{(\mathbf{a},\mathbf{a})_{\mathbf{C}}}$. The Hermitian angle is limited to the first quadrant such that $0 \leq \Theta_{\mathbf{H}} \leq \pi/2$. The directional estimation error in spatial frequency domain, $\epsilon_\theta(\bar{\omega})$, can then be expressed as

$$\epsilon_\theta(\overline{\omega}) = \Theta_{\mathbf{H}}\left\{j\overline{\omega}P(\overline{\omega}), \mathbf{U}^{+}\mathbf{P}_\Delta\right\}. \quad (26)$$

Fig. 4 shows the directional estimation error for cubic, tetrahedral, body-centered cubic (BCC), and cubic close-packed (CCP) topologies with unit spatial sampling period, $r = 1$, at $\|\overline{\omega}\| = \pi/4$. It may be observed that the directional estimation error of the tetrahedral mesh topology is greater than those of other topologies almost by an order of magnitude. The directional estimation error of cubic and BCC topologies are very similar. The CCP topology has the highest accuracy, particularly for horizontal directions.

Table I shows the averages, maxima, and standard deviations of directional estimation errors for different topologies. It may be observed that the directional accuracy of cubic, CCP, BCC topologies are comparable, but the tetrahedral topology has a lower directional accuracy than the others. Average and maximum angular errors for the cubic, CCP, BCC topologies are less than 1°, and 2.5°, respectively. Maximum directional estimation error on a tetrahedral mesh can be as high as 19°. This result shows that the tetrahedral mesh is not suitable for directional estimation of simulated sound fields. Cubic topology provides a good trade-off between accuracy and computational requirements.

TABLE I
MEAN ($\bar{\epsilon}_\theta$), MAXIMUM ($\max\{\epsilon_\theta\}$), AND STANDARD DEVIATION (σ_θ) OF DIRECTIONAL ESTIMATION ERROR IN DEGREES.

	Cubic	Tetra.	BCC	CCP
$\bar{\epsilon}_\theta$	0.92°	8.10°	0.61°	0.57°
$\max\{\epsilon_\theta\}$	2.22°	19.01°	1.49°	2.45°
σ_θ	0.51°	3.71°	0.34°	0.46°

IV. SIMULATION OF MICROPHONE DIRECTIVITY IN DWM MODELS

A. Microphone directivity in DWM models

Microphones have different sensitivities to sound waves incident from different directions. The ratio which quantifies this sensitivity difference is called the microphone's *directivity function* and is denoted as $\Gamma(\theta, \phi)$. More specifically,

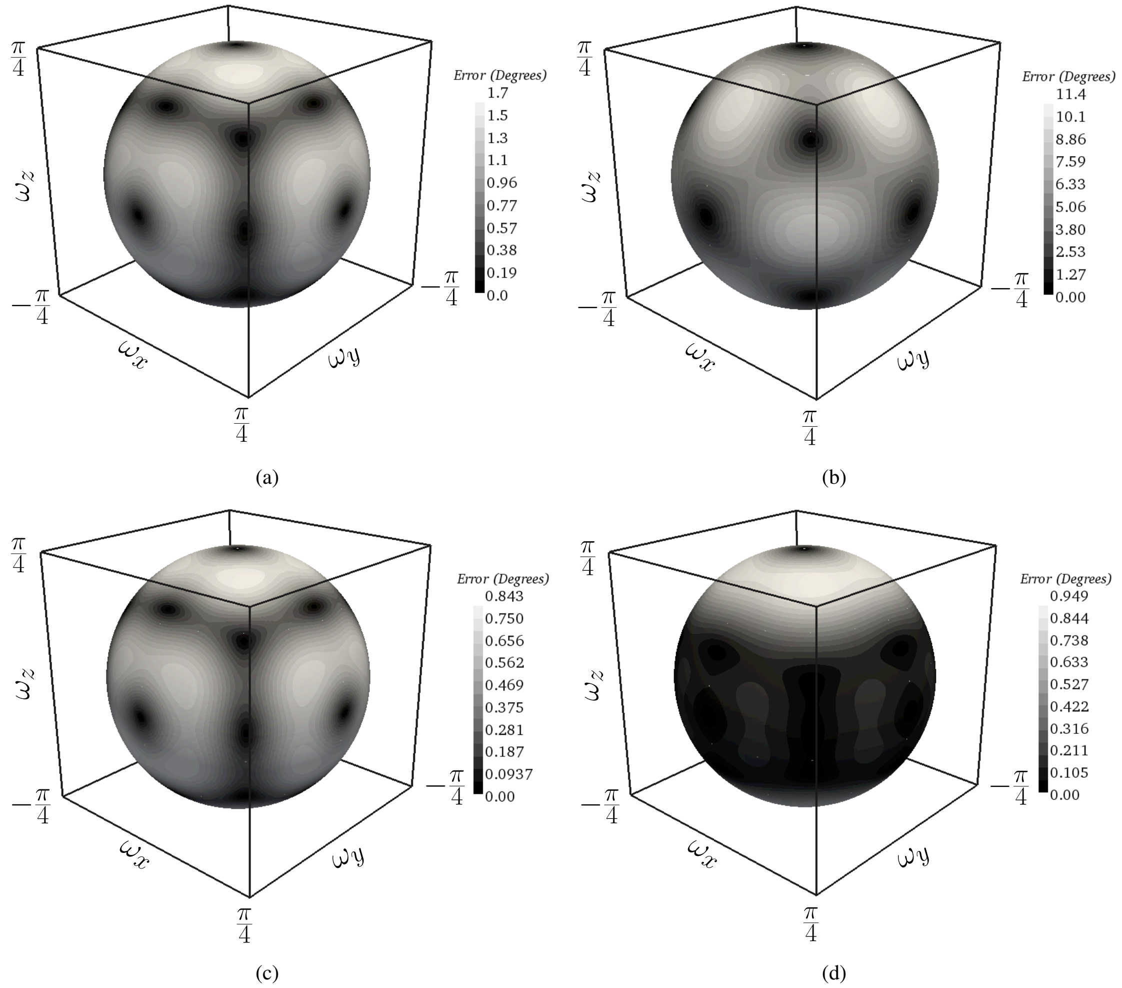

Fig. 4. The directional estimation error, ϵ_θ, with $\|\overline{\omega}\| = \pi/4$ for (a) cubic, (b) tetrahedral, (c) body-centered cubic (BCC), and (d) cubic close-packed (CCP) topologies.

microphone directivity represents the ratio of a microphone's response for a plane wave incident from a given direction, to its response for a plane wave incident from its look direction. It can be expressed as the ratio of the rms energy of the microphone's output voltage for a plane wave incident from an arbitrary direction, $v_m(\theta, \phi, t)$, to the rms energy of output for a plane wave with the same total energy incident from the front direction, $v_m(0, 0, t)$, such that:

$$\Gamma(\theta, \phi) = \sqrt{\frac{\int_T^{T+\Delta T} v_m(\theta, \phi, t)^2 dt}{\int_T^{T+\Delta T} v_m(0, 0, t)^2 dt}}. \tag{27}$$

In a complex sound field such as a room, the sound field can be expressed as a superposition of many plane waves incident from different directions. Let us consider the case where there are K plane waves, $p_k(t)$. Pressure, particle velocity, and instantaneous intensity at the microphone position are:

$$p(\mathbf{x}, t) = \sum_{k=1}^{K} p_k(t), \tag{28}$$

$$\mathbf{v}(\mathbf{x}, t) = \frac{1}{\rho c} \sum_{k=1}^{K} p_k(t) \hat{n}_k, \tag{29}$$

$$\mathbf{I}(\mathbf{x}, t) = \frac{1}{\rho c} \sum_{i=1}^{K} \sum_{k=1}^{K} p_i(t) p_k(t) \hat{n}_k, \tag{30}$$

where $\hat{n}_k$ is the propagation direction of each plane wave. The energy flow will have a direction coincident with the instantaneous intensity showing the instantaneous direction of the sound field at the given position, $\mathbf{x}$. It may be observed that the directions of the instantaneous intensity and particle velocities of individual plane waves are related in a complex way.

In a stationary sound field, the squared output signal of a directional microphone with an acoustical axis in the (Θ, Φ) direction, is proportional to the weighted intensity field integrated over a unit sphere [36] such that

$$|v_m(\Theta, \Phi)|^2 \propto \int_0^{2\pi} \int_0^{\pi} I(\theta, \phi) |\Gamma(\Theta - \theta, \Phi - \phi)|^2 \sin\phi d\phi \, d\theta. \tag{31}$$

Here, $I(\theta, \phi)$ is the directional distribution of intensity that can be expressed in terms of the time-dependent directional distribution of energy, $E(\theta, \phi, t)$ as

$$I(\theta, \phi) = \int_0^{\infty} E(\theta, \phi, t) dt. \tag{32}$$

The relation between the total acoustic energy in the sphere, E, and the time-dependent directional distribution of energy is defined as

$$d^3E = E(\theta, \phi, t)\, dt\, d\Omega, \tag{33}$$

where $d\Omega$ represents an infinitesimal solid angle. Then, the instantaneous squared output signal of the microphone is proportional to the weighted rate of change of energy in the unit sphere:

$$|v(\Theta, \Phi, t)|^2 \propto \int_0^{2\pi}\int_0^{\pi} E(\theta, \phi, t)|\Gamma(\Theta - \theta, \Phi - \phi)|^2 \sin\phi d\phi\, d\theta. \tag{34}$$

Due to the acoustic-energy corollary [37], the rate of change of acoustic energy in a volume can be expressed using the intensity distribution on a surface, S, enclosing that volume, such that:

$$\frac{dE}{dt} = \int_S [-\mathbf{I}(t) \cdot \hat{\mathbf{u}}_r]\, d\mathrm{S}. \tag{35}$$

where $\hat{\mathbf{u}}_r$ is the outward unit vector normal to the surface. The case where $\mathbf{I} \cdot \hat{\mathbf{u}}_r < 0$, corresponds to an energy entering the volume and the case where $\mathbf{I} \cdot \hat{\mathbf{u}}_r > 0$ corresponds to energy leaving the volume. The time dependent directional distribution of energy can be expressed as the instantaneous energy flow through the surface from the given direction such that:

$$E(\theta, \phi, t) = -\mathbf{I}(\theta, \phi, t) \cdot \hat{\mathbf{u}}_r(\theta, \phi). \tag{36}$$

It is then possible to express the relation between the output of a directional microphone and the instantaneous intensity as:

$$|v_m(\Theta, \Phi, t)|^2 \propto \iint_S [-\mathbf{I}(\theta, \phi, t) \cdot \hat{\mathbf{u}}_r(\theta, \phi)]\, |\Gamma(\Theta - \theta, \Phi - \phi)|^2 \sin\phi d\phi d\theta. \tag{37}$$

In other words, the squared output of the microphone is proportional to the weighted net energy flow.

Previous work on simulation of microphones on DWMs investigated differential microphone arrays [11]. The simplest example for differential microphone arrays is the first-order microphone consisting of two spatially separated omnidirectional microphone capsules [38]. In order for these microphones to provide the intended directional response for a wide frequency range, the separation between the microphones should be small. Simulation of these first-order differential arrays on DWM models is not always possible as the minimum separation between individual microphones cannot be smaller than the spatial sampling period, r, as given in (6). For example, at the typical mesh update rate of $f_S = 44.1$kHz, two simulated capsules cannot be positioned any closer than $r \approx 1.35$cm to each other. In addition, the simulated microphones can only be positioned at fixed orientations determined by the mesh topology. Theoretically, it may be possible to overcome this limitation by using an oversampled DWM model. However, in practice, the computational requirements of an oversampled 3D DWM model would increase cubically with decreasing spatial sampling period, r. Therefore, we assume that the microphones simulated in DWM models are *point-like*. With this assumption, the instantaneous intensity vector at the junction represents the instantaneous net energy flow and the direction of the sound field. Therefore, the integral over the surface enclosing the microphone is reduced to a single term,

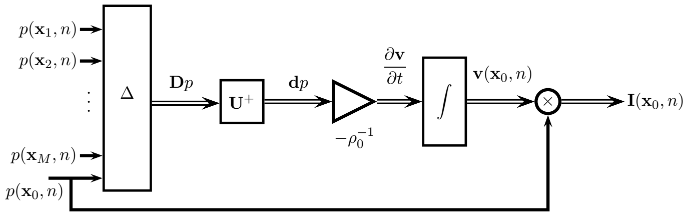

Fig. 5. The processing stages for calculating the instantaneous intensity, $\mathbf{I}(\mathbf{x}_0, n)$ at a junction from the pressure values, $p(\mathbf{x}_i)$ at the DWM junctions using the inverse projection matrix, $\mathbf{U}^+$, inverse of the ambient density, ρ_0^{-1}, and a discrete time integrator.

$$|v_m(\Theta, \Phi, n)|^2 \propto |\mathbf{I}(\mathbf{x}, n)||\Gamma(\Theta - \theta_n, \Phi - \phi_n)|^2, \tag{38}$$

where (θ_n, ϕ_n) denotes the direction of the instantaneous intensity vector, $\mathbf{I}(n)$.

As discussed in the previous section, it is possible to obtain an approximation of the instantaneous acoustic intensity at a DWM junction. The magnitude of the microphone's output signal can thus be calculated. However, the polarity of the signal should be imposed on this magnitude to obtain useful results. For practical purposes, we assume that the output of the microphone and the pressure recorded at the microphone position are in-phase. Therefore, the polarity of the output voltage can be restored from the sign of the pressure as

$$v_m(n) = \mathrm{sgn}\,[p(n)]\,|v_m(n)|, \tag{39}$$

where $\mathrm{sgn}\,[\bullet]$ is the sign function. It should be noted that due to the point-like receiver assumption, the sound field is assumed to have a single wave component whose direction changes at each iteration. In other words, the method does not distinguish between the individual wave components that together make up the sound field. While this approach is not suitable for pressure gradient directional microphones composed of multiple elements, it is well-justified for single diaphragm directional microphones.

Microphone directivity changes with frequency. It is generally tabulated in octave or $1/3$-octave band resolution. Therefore, the directional weighting operation discussed above should be carried out at all frequency bands where directivity function is defined. Microphones also have direction-independent frequency responses called the *diffuse field response*. A filter modeling the diffuse field response should be incorporated into the simulation in order to obtain a more accurate result.

B. Implementation

The proposed method can be implemented as an efficient algorithm. Fig. 5 shows how instantaneous intensity is calculated from the pressure values at the given junction and its neighbors. The pressure difference vector $\mathbf{D}p(\mathbf{x}_0, n)$ is obtained by subtracting the central junction pressure from the pressure values of neighboring junctions and dividing these terms by the spatial sampling period as described in (13). The approximation of the pressure gradient $\mathbf{d}p(\mathbf{x}_0, n)$ is obtained by multiplying the difference vector by the inverse projection matrix $\mathbf{U}^{+}$. The result is scaled by the negative inverse of the ambient density, ρ_0, and integrated using a discrete-time integrator having a transfer function $H_{int}(z) = \frac{Tz^{-1}}{1-z^{-1}}$ where $T = 1/f_S$ is the temporal sampling period. The obtained vector is an approximation of the instantaneous particle velocity $\mathbf{v}(\mathbf{x}_0, n)$ at the central junction. The instantaneous intensity $\mathbf{I}(\mathbf{x}_0, n)$ is obtained by multiplying the velocity and the pressure.

The impulse response recorded by a simulated directional microphone can be calculated using the instantaneous intensity and pressure values at the junction for an impulsive excitation as shown in Fig. 6. First, the magnitude and direction of the instantaneous intensity vector are calculated. The magnitude of the instantaneous intensity, $|\mathbf{I}(\mathbf{x}_0, n)|$ is weighted by the squared value of directivity functions, $|\Gamma_C(\theta, \phi)|^2$ at each frequency band according to the instantaneous direction of incidence, (θ_n, ϕ_n). The square-root of the obtained value is multiplied with the sign of pressure and filtered by the corresponding octave-band filter, $H_C(z)$. The results from each frequency band are added and the result is filtered by the diffuse-field filter, $H_d(z)$ to obtain the directional impulse response. Zero-phase filtering may be used to prevent the phase distortions associated with the octave-band and diffuse field filters.

The microphone directivity patterns, $\Gamma_C(\theta, \phi)$ can be stored as piecewise polynomials (i.e. shape preserving splines) or as polynomials of harmonic functions. This way it is possible to rotate the look direction of the virtual microphone easily. Thus, a directional gain for each frequency band can be obtained from these functions for any direction of incidence and for any microphone rotation.

V. EXAMPLE: A CARDIOID MICROPHONE

A. Simulation of the microphone in a DWM-based room model

For the purpose of demonstrating the method, a studio microphone, AKG C 214 is simulated. AKG C 214 is a single capsule, large diaphragm cardioid microphone. A 3D DWM model of a rectangular enclosure of size 4.1 m×5 m×2.1 m with a cubic mesh topology was implemented. The update rate of the mesh was $f_S = 44.1$ kHz, and the theoretical upper bound for the mesh bandwidth was 11025 Hz. The spatial sampling period, which corresponds to the distance between the junctions was $r \approx 1.35$cm according to (6). The absorption coefficients of the walls and the ceiling were selected as $\alpha = 0.6461$, and the floor as $\alpha = 0.4$ so that the reverberation time of the enclosure is $\mathrm{T}_{60} = 150$ ms according to Sabine's equation [33]. The reflecting surfaces were modeled as phase-inverting 1D boundaries (i.e. each boundary junction had one neighbour). The horizontal plane directivity patterns and diffuse field response of the microphone were obtained from microphone specifications [39]. The data from available directivity plots representing, $|\Gamma(\theta, \phi)|^2$ were fitted with shape-preserving piecewise cubic spline functions. Fig. 7 shows the fitted directivity functions. The diffuse field response of the

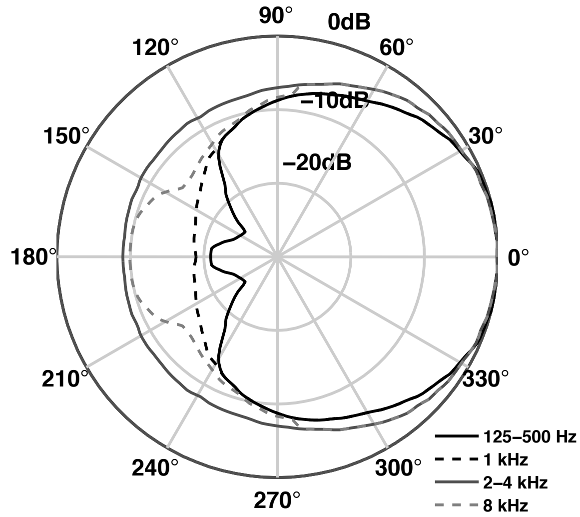

Fig. 7. Shape-preserving cubic spline functions fitted to tabulated directivity plots representing the squared directivity function, $|\Gamma_C(\theta, \phi)|^2$, of the AKG C 214 microphone at octave bands with center frequencies from $f_C = 125$ Hz to $f_C = 8$ kHz.

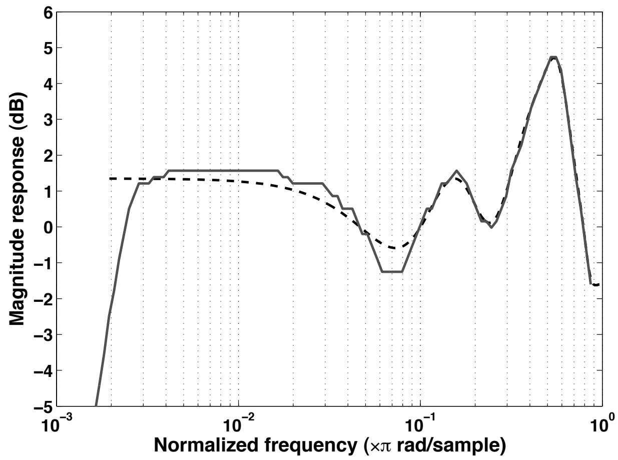

Fig. 8. Magnitude spectra of the diffuse field response of the AKG C 214 microphone (solid curve) and the 10^{th} order minimum-phase IIR filter modeling this response (dashed curve).

microphone was modeled using a 10^{th} order, minimum-phase IIR filter designed using the Yule-Walker method (see Fig. 8).

It was assumed that the directivity function has rotational symmetry around its look direction. Therefore, instead of obtaining azimuth and elevation angles separately, it is possible to use the angle, ψ_n between the intensity vector, $\hat{\mathbf{I}}$, and the look direction vector, $\hat{\mathbf{u}}_m$, such that:

$$\psi_n = \arccos\left(\frac{\hat{\mathbf{I}} \cdot \hat{\mathbf{u}}_m}{\|\mathbf{I}\|}\right), \tag{40}$$

where $\hat{\mathbf{u}}_m = [\cos\Theta\cos\Phi \quad \sin\Theta\cos\Phi \quad \sin\Phi]$. This makes it possible to use the horizontal directivity pattern of the microphone for all elevation angles.

The DWM model was excited with a symmetric trivariate Gaussian pulse, modeling an isotropic pressure distribution

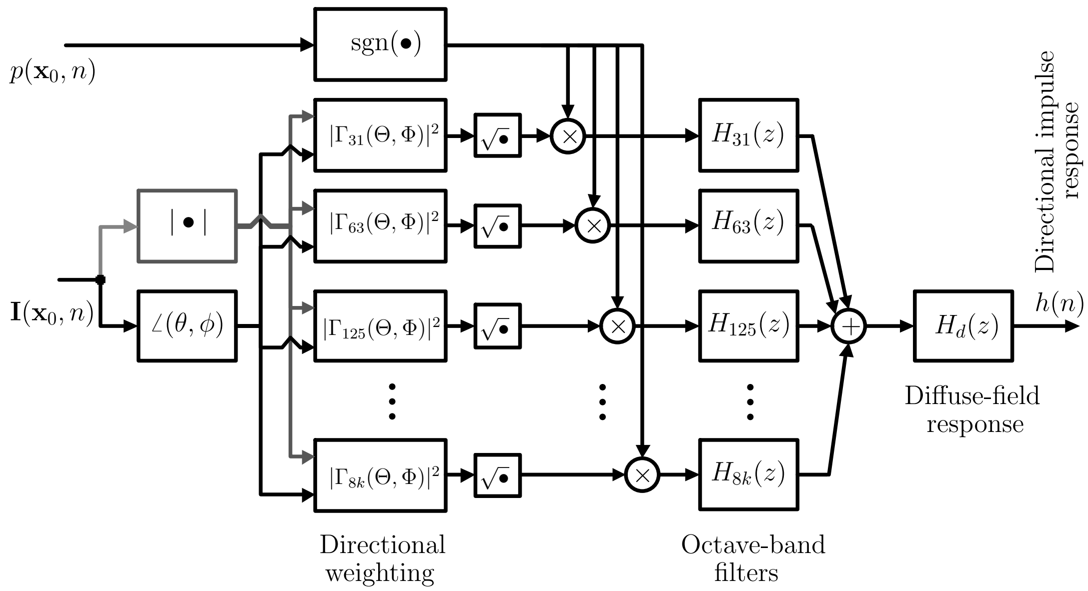

Fig. 6. The block diagram showing the processing stages to find the instantaneous direction of incidence at a junction.

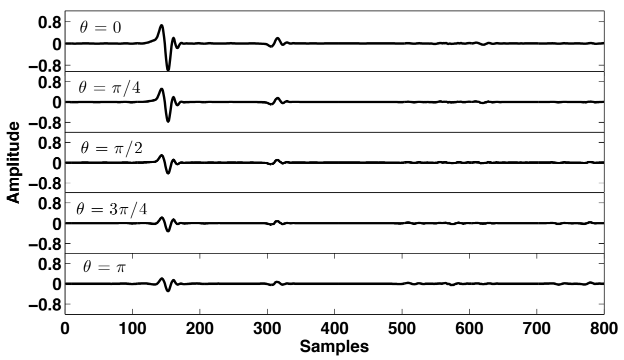

Fig. 9. Impulse responses in the modeled enclosure using microphone orientations of $\theta = 0,\ \pi/4,\ \pi/2,\ 3\pi/4,\ \pi$.

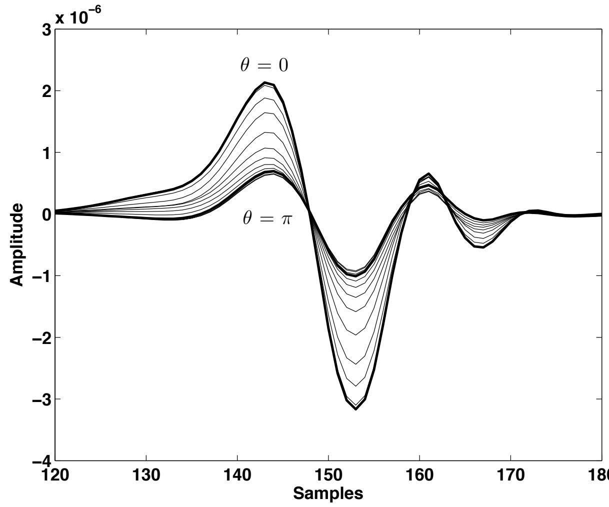

Fig. 10. Direct sound as captured by the simulated AKG C 214 microphone for 13 different orientations of the microphone between 0 and π with an interval of $\pi/12$ radians.

around the point of excitation. The pulse was positioned at the center of the model ($x = 2.05$ m, $y = 2.50$ m, $z = 1.05$ m), and had a variance of 4 spatial samples. The model was iterated 4410 times to obtain the first 100 ms of the pressure values and the pressure gradients at the junction positioned at, $x = 2.05$ m, $y = 1.35$ m and $z = 1.05$ m. The proposed method was applied as an offline post-processing stage to obtain the impulse response registered by the simulated microphone.

Fig. 9 shows the first 800 samples of the impulse response as registered by the simulated cardioid microphone with different rotations from $\theta = 0$ (i.e. facing the sound source) to $\theta = \pi$ (i.e. facing away). It may be observed that as the simulated microphone faces away from the source, the amplitude of the direct sound (between 120 and 180 samples) decreases. On the other hand reflection from the back wall is captured at a greater amplitude (between 700 and 760 samples) when the cardioid is facing that wall.

Fig. 10 shows the portion of the impulse response containing the direct wavefront as captured by the simulated cardioid microphone. The figure contains the impulse response between 120 and 180 samples for microphone rotations on the horizontal plane with $\pi/12$ radians separation. The response with the maximum amplitude belongs to the case where the microphone is facing the source and the minimum amplitude to the case where the simulated microphone facing away. It may be observed that as the simulated microphone is rotated to face away from the source, the amplitude of the microphone output signal decreases. This situation is reversed for the reflection from the back wall as may be observed in Fig. 11. Here, the reflection from the back wall is captured with higher amplitude by the microphone facing that wall. Also, note the scale difference between the two plots.

TABLE II
MAXIMUM AND MEAN ERRORS (IN dB) BETWEEN THE INTENDED DIRECTIVITY FUNCTION, $|\Gamma_C(\theta,\phi)|$, AND SIMULATED RESULTS AT DIFFERENT OCTAVE BANDS.

f_C	125 Hz	250 Hz	500 Hz	1 kHz	2 kHz	4 kHz	8 kHz
Max. error	3.16	0.29	1.75	1.66	0.23	0.70	3.48
Mean error	0.75	0.07	0.38	0.55	0.11	0.35	1.68

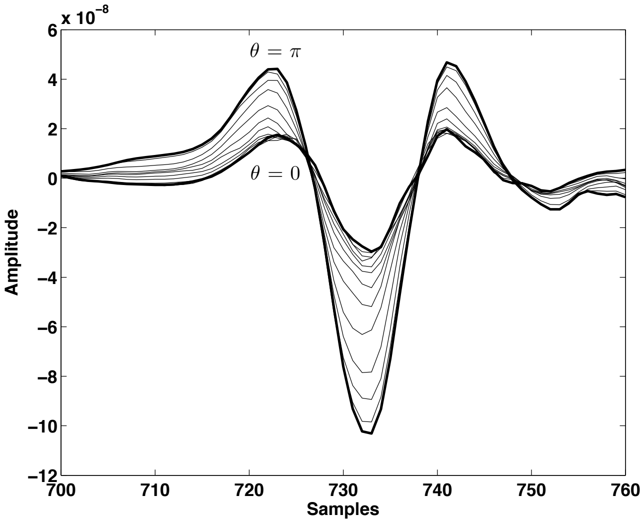

Fig. 11. Reflection from the back wall as captured by the simulated AKG C 214 microphone for 13 different orientations of the microphone between 0 and π with an interval of $\pi/12$ radians.

B. Directional accuracy of the method

For evaluating the directional accuracy of the proposed method another set of simulations were carried out. The microphone position was designated as the center of the same DWM model used in Sec. V-A. Source positions were designated with 10° azimuth separation at 1 m distance from the microphone position . The mesh was sequentially excited using Gaussian pulses with a variance of 4 samples positioned at these source locations. The pressure and velocity components were obtained for the first 200 iterations of each run representing the direct portion of the sound field. The corresponding directional responses of the microphone were obtained using the proposed method. These responses were filtered using octave-band filters. Energy for each direction was calculated and normalized with respect to the energy at the front direction in order to obtain the directive sensitivity of the simulated microphone.

Fig. 12 shows the squared directivity function, $|\Gamma_C(\theta,\phi)|^2$ at different octave-bands, along with the normalized energy of the simulated signal for the tested directions. It may be observed that, except for the octave band with 8 kHz center frequency, the simulation results follow the original directivity pattern very closely. Table II shows the maximum and mean absolute errors at different octave bands. The results suggest that the proposed method is capable of accurately simulating microphone directivity in 3D DWM models. The accuracy of the method is worse for 8 kHz octave band due to direction dependent dispersion that occur more prominently at that frequency range. It should be noted that the errors given in the table are half of the errors plotted in Fig. 12 as the tabulated values are calculated as the difference between the rms energy and the magnitude of the directivity function, $|\Gamma(\theta,\phi)|$.

VI. CONCLUSIONS

A method for simulating directional microphones in 3D digital waveguide mesh (DWM) based models of room acoustics was presented in this paper. The proposed method is based on the calculation of the intensity vector at a given junction in a DWM by using the pressure and the velocity components of the simulated sound field. A numerical method for the calculation of instantaneous intensity on DWM models was given. The accuracies of different mesh topologies for the estimation of the direction of intensity vectors were analyzed. It was found that the directional accuracies of cubic, body-centered cubic (BCC), and cubic close-packed (CCP) topologies are comparable. The tetrahedral topology had the worse accuracy. The relationship between instantaneous intensity and microphone directivity was discussed. It was shown that instantaneous intensity can be used in simulating directional microphones if the microphone is assumed to be point-like.

A virtual directional microphone positioned in a DWM-based acoustical model of a rectangular room was given as a practical example. The 3D DWM model of a medium sized room was excited with an omnidirectional pulse. The proposed method was applied with the cardioid directivity patterns of a real microphone. The results were presented for various rotations of the microphone. Further simulations were also presented to demonstrate the directional accuracy of the method. Cubic mesh topology was used in the example as it provides an excellent trade-off between accuracy and computational complexity. However, it is possible to use other mesh topologies easily with the proposed method.

Room acoustics simulation using geometrical models are widely used in research and in practice. Although these models are computationally less demanding than DWMs, they do not provide physically accurate simulations of wave propagation in rooms. The advances in computer hardware will make it possible in the near future to simulate huge acoustic models with wave-theoretical, numerical models such as DWMs. The method proposed in this paper is a useful step towards achieving a more complete room acoustic simulation with such models. It would also be a useful tool for applications where an accurate simulation of room acoustics is essential. Three particular examples are simulation of microphone arrays, simulation of spatial audio systems, and auralization of room acoustics.

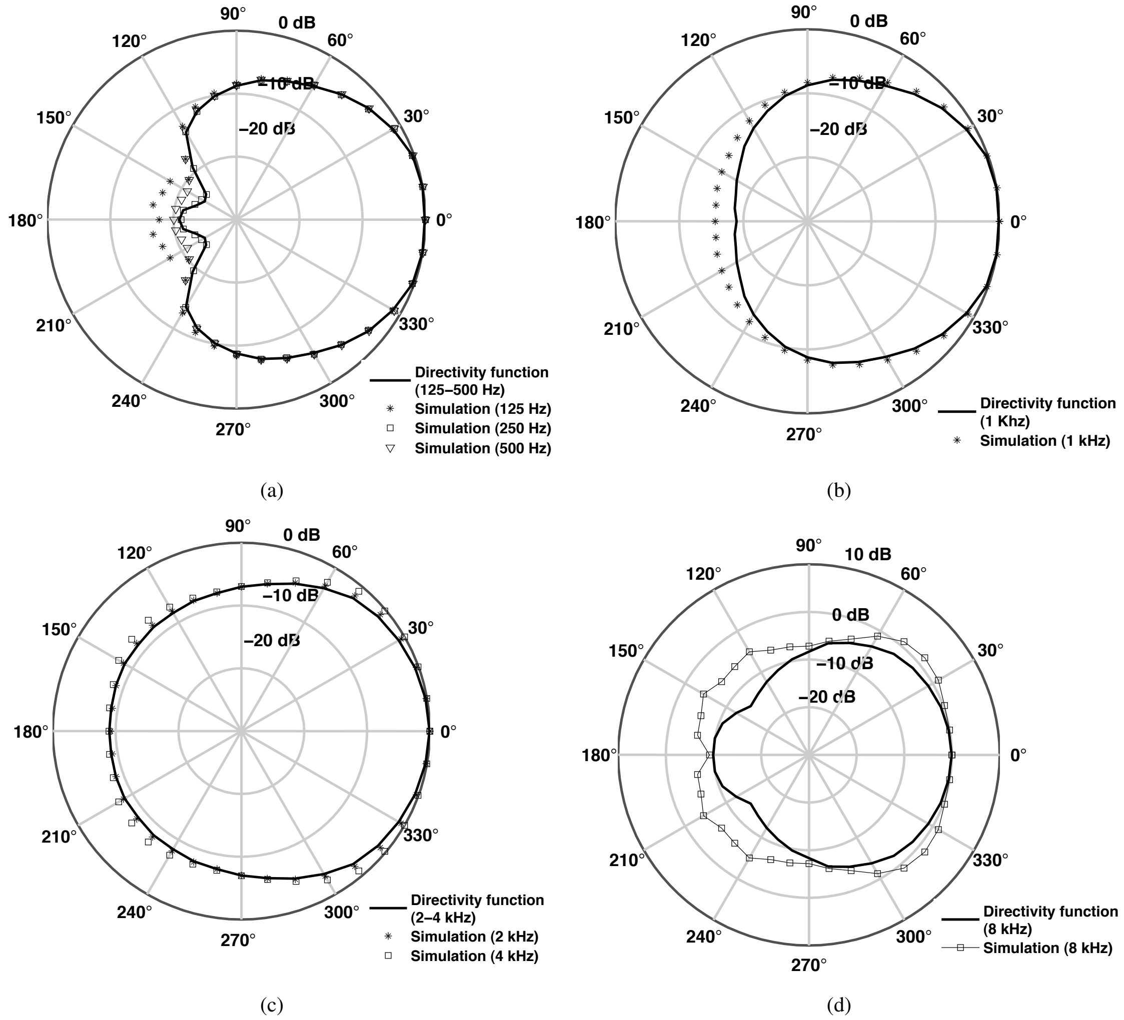

Fig. 12. The directivity of the simulated microphone and the intended directivity pattern at octave bands with center frequencies (a) 125, 250, and 500 Hz, (b) 1 kHz, (c) 2kHz and 4kHz, and (d) 8kHz. The solid curves denote the intended directivity. The markers denote the simulation results. Note the scale difference for the 8kHz octave band.

Acknowledgment

The authors would like to thank the anonymous reviewers for their constructive comments. The first and third authors are funded by the Engineering and Physical Sciences Research Council (EPSRC) Research Grant EP/F001142/1. The second author is funded by VISNET II, a European Network of Excellence (http://www.visnetnoe.org), under the European Commission IST FP6 programme.

References

[1] S. Bilbao, *Wave and scattering methods for numerical simulation*. Chichester, UK: John Wiley & Sons, 2004.

[2] D. T. Murphy and M. J. Beeson, "Modelling spatial sound occlusion and diffraction effects using the digital waveguide mesh," in *Proc. AES* 24^{th} *Conference on Multichannel Audio*, Banff, Alberta, Canada, 2003, pp. 207–216.

[3] P. Svensson and U. R. Kristiansen, "Computational modeling and simulation of acoustic spaces," in *Proc. of AES* 22^{nd} *Int. Conf. on Virtual, Synthetic and Entertainment Audio (AES22)*, Espoo, Finland, June 15-17 2002, pp. 11–30.

[4] M. Vörländer, *Auralization - Fundamentals of Acoustics, Modelling, Simulation, Algorithms and Acoustic Virtual Reality*. Springer-Verlag, 2008.

[5] L. Savioja, T. Rinne, and T. Takala, "Simulation of room acoustics with a 3-D finite difference mesh," in *Proc. Int. Comp. Music Conf. (ICMC'94)*, Aarhus, Denmark, September 1994, pp. 463–466.

[6] D. T. Murphy and D. M. Howard, "Modelling and directionally encoding the acoustics of a room," *Electronics Lett.*, vol. 34, no. 9, pp. 864–865, April 1998.

[7] L. Savioja and V. Välimäki, "Interpolated rectangular 3-D digital waveguide mesh algorithms with frequency warping," *IEEE Trans. on Speech and Audio Process.*, vol. 11, no. 6, pp. 783–790, November 2003.

[8] H. Hacıhabiboğlu, B. Günel, and A. M. Kondoz, "Source directivity simulation in digital waveguide mesh-based room acoustics models," in *Proc. AES* 30^{th} *Int. Conf. on Intelligent Audio Environments*, Saariselkä, Finland, March 15-17 2007, pp. (CD–ROM).

[9] ——, "Time-domain simulation of directive sources in 3-D digital waveguide mesh-based acoustical models," *IEEE Trans. on Audio, Speech and Language Process.*, vol. 16, no. 5, pp. 934–946, July 2008.

[10] J. Escolano, J. J. López, and B. Pueo, "Directive sources in acoustic discrete-time domain simulations based on directivity diagrams," *J. Acoust. Soc. Am.*, vol. 121, no. 6, pp. EL256–EL262, June 2007.

[11] A. Southern and D. Murphy, "Methods for 2nd order spherical harmonic spatial encoding in digital waveguide mesh virtual acoustic simulations," in *Proc. of 2007 IEEE Workshop on Applications of Signal Processing to Audio and Acoustics (WASPAA'07)*, New Paltz, NY, USA, October 21-24 2007, pp. 203–206.

[12] A. Southern and D. T. Murphy, "A second order differential microphone technique for spatially encoding virtual room acoustics," Presented at the AES 124th Convention, Preprint #7332, Amsterdam, Netherlands, May 17-20 2008.

[13] A. Craggs, "Acoutical modeling: Finite element method," in *Handbook of Acoustics*, M. J. Crocker, Ed. Wiley-Interscience, 1998, ch. 12, pp. 149–156.
[14] A. F. Seybert and T. W. Wu, "Acoustic modeling: Boundary element methods," in *Handbook of Acoustics*, M. J. Crocker, Ed. Wiley-Interscience, 1998, ch. 13, pp. 157–167.
[15] D. Botteldooren, "Acoustical finite-difference time-domain simulation in a quasi-Cartesian grid," *J. Acoust. Soc. Am.*, vol. 95, no. 5, pp. 2313–2319, May 1994.
[16] ——, "Finite-difference time-domain simulation of low-frequency room acoustic problems," *J. Acoust. Soc. Am.*, vol. 98, no. 6, pp. 3302–3308, December 1995.
[17] J. C. Strikwerda, *Finite Difference Schemes and Partial Differential Equations*, 2nd ed. Philadelphia, PA, USA: Society for Industrial and Applied Mathematics, 2004.
[18] K. Karplus and A. Strong, "Digital synthesis of plucked-string and drum timbres," *Computer Music J.*, vol. 7, no. 2, pp. 43–55, Summer 1983.
[19] J. O. Smith, III, "Physical modeling using digital waveguides," *Computer Music J.*, vol. 16, no. 4, pp. 74–91, Winter 1992.
[20] ——, "Principles of digital waveguide models of musical instruments," in *Applications of digital signal processing to audio and acoustics*, M. Kahrs and K. Brandenburg, Eds. New York, USA: Kluwer Academic Publishers, 2002, pp. 417–466.
[21] V. Välimäki, J. Pakarinen, C. Erkut, and M. Karjalainen, "Discrete-time modelling of musical instruments," *Reports on Progress in Physics*, vol. 69, pp. 1–78, January 2006.
[22] J. Mullen, D. M. Howard, and D. T. Murphy, "Acoustical simulations of the human vocal tract using 1D and 2D digital waveguide software model," in *Proc.* 7^{th} *Int. Conf. on Digital Audio Effects (DAFX'04)*, Napoli, Italy, October 5-8 2004, pp. 311–314.
[23] ——, "Real-time dynamic articulations in the 2-D waveguide mesh vocal tract model," *IEEE Trans. on Audio, Speech and Language Process.*, vol. 15, no. 2, pp. 577–585, February 2007.
[24] S. A. Van Duyne and J. O. Smith, III, "The 2-D digital waveguide mesh," in *Proc. of 1993 IEEE Workshop on Applications of Signal Processing to Audio and Acoustics (WASPAA'93)*, New Paltz, NY, USA, 17-20 October 1993, pp. 177–180.
[25] J. Laird, P. Masri, and C. N. Canagarajah, "Efficient and accurate synthesis of circular membranes using digital waveguides," in *IEE Colloquium on Audio and Music Technology: The Challenge of Creative DSP*, London, UK, 18 November 1998, pp. 12/1–12/6.
[26] A. Kelloniemi, V. Välimäki, and L. Savioja, "Simulation of room acoustics using 2-D digital waveguide meshes," in *Proc. 2006 IEEE Int. Conf. on Acoustics, Speech and Signal Processing (ICASSP'06)*, vol. 5, Toulouse, France, May 15-19 2006, pp. 313–316.
[27] S. A. Van Duyne and J. O. Smith, III, "The tetrahedral digital waveguide mesh," in *Proc. of 1995 IEEE Workshop on Applications of Signal Processing to Audio and Acoustics (WASPAA'95)*, New Paltz, NY, USA, 15-18 October 1995, pp. 234–237.
[28] M. van Walstijn and K. Kowalczyk, "On the numerical solution of the 2d wave equation with compact FDTD schemes," in *Proc.* 11^{th} *Int. Conf. on Digital Audio Effects (DAFx-08)*, Espoo, Finland, 1-4 September 2008, pp. 205–212.
[29] G. R. Campos and D. M. Howard, "On the computational efficiency of different waveguide mesh topologies for room acoustics simulation," *IEEE Trans. on Speech and Audio Process.*, vol. 13, no. 5, pp. 1063–1072, September 2005.
[30] S. Bilbao and J. O. Smith, III, "Finite difference schemes and digital waveguide networks for the wave equation: Stability, passivity, and numerical dispersion," *IEEE Trans. on Speech and Audio Processing*, vol. 11, no. 3, pp. 255–266, May 2003.
[31] G. Campos and D. M. Howard, "On the computation time of three-dimensional digital waveguide mesh acoustic models," in *Proc.* 26^{th} *Euromicro Conf.*, Maastricht, Netherlands, 5-7 September 2000, pp. 332–339.
[32] H. Hacıhabiboğlu, B. Günel, and A. M. Kondoz, "On the accuracy of first-order numerical derivatives in multidimensional digital waveguide mesh topologies," *IEEE Signal Process. Lett.*, vol. 15, pp. 9–12, January 2008.
[33] A. D. Pierce, *Acoustics: An introduction to its physical principles and applications*. Woodbury, NY, USA: Acoustical Society of America, 1994.
[34] L. Savioja and V. Välimäki, "Reducing the dispersion error in the digital waveguide mesh using interpolation and frequency-warping techniques," *IEEE Trans. on Speech and Audio Processing*, vol. 8, no. 2, pp. 184–194, March 2000.
[35] K. Scharnhorst, "Angles in complex vector spaces," *Acta Applicandae Mathematicae*, vol. 69, no. 1, pp. 95–103, October 2001.
[36] H. Kuttruff, *Room Acoustics*, 4th ed. London, UK: SPON Press, 2000.
[37] F. Jacobsen, "Sound intensity," in *Springer Handbook of Acoustics*, T. Rossing, Ed. New York, USA: Springer Science+Business Media LLC, 2007, pp. 1053–1975.
[38] G. W. Elko, "Differential microphone arrays," in *Audio signal processing for next-generation multimedia communication systems*, Y. Huang and J. Benesty, Eds. Boston, USA: Kluwer Academic Publishers, 2004, pp. 11–65.
[39] AKG Acoustics GmbH. AKG C 214 Microphone Specifications. [Online]. Available: http://www.akg.com

Hüseyin Hacıhabiboğlu (S'96-M'00) was born in Ankara, Turkey, in 1978. He received the B.Sc. (Hons.) degree from the Middle East Technical University, Ankara, Turkey, in 2000, the M.Sc. degree from the University of Bristol, U.K., in 2001, both in electrical and electronic engineering, and the Ph.D. degree in computer science from Queens University Belfast, U.K., in 2004. Between 2004-2008, he was with the Multimedia and DSP Research Group (I-Lab) at the Centre for Communication Systems Research (CCSR), University of Surrey, U.K.

Currently he is with the Centre for Digital Signal Processing Research (CDSPR), Division of Engineering, King's College London, U.K. His research interests include audio signal processing, room acoustics modeling and simulation, multichannel audio systems, psychoacoustics of spatial hearing, and microphone array processing.

Dr. Hacıhabiboğlu is a member of the Audio Engineering Society (AES), Turkish Acoustics Society (TAD), and the European Acoustics Association (EAA).

Banu Günel (S'97-M'00) was born in Antalya, Turkey, in 1977. She received the B.Sc. (Hons) degree in electrical and electronic engineering from the Middle East Technical University, Ankara, Turkey, in 2000, the M.Sc. degree in communication systems and signal processing from the University of Bristol, U.K., in 2001, and the Ph.D. degree on audio and acoustical signal processing from the Queens University of Belfast, U.K., in 2004.

Since 2004, she has been working as a Research Fellow in the Centre for Communication Systems Research (CCSR) at the University of Surrey, U.K. Her main research interests are spatial audio, array signal processing, acoustic imaging, psychoacoustics, and communication acoustics.

Dr. Günel is a member of the European Acoustics Association (EAA) and the Audio Engineering Society (AES).

Zoran Cvetković (SM'04) received his Dipl.Ing.El. and Mag.El. degrees from the University of Belgrade, Yugoslavia, in 1989 and 1992, respectively; the M.Phil. from Columbia University in 1993; and the Ph.D. in electrical engineering from the University of California, Berkeley, in 1995. He held research positions at EPFL, Lausanne, Switzerland (1996), and at Harvard University (2002-04). Between 1997 and 2002 he was a member of the technical staff of AT&T Shannon Laboratory. He is now Reader in Signal Processing at King's College London. His research interests interests are in the broad area of signal processing, ranging from theoretical aspects of signal analysis to applications in source coding, telecommunications, and audio and speech technology.